Dalton Transactions

Accepted Manuscript

This article can be cited before page numbers have been issued, to do this please use: M. Richert, M. Walczyk, M. Cieslak, J. Kazmierczak-Baranska, K. Krolewska, G. Wrzeszcz, T. Muzio and S. Biniak, *Dalton Trans.*, 2019, DOI: 10.1039/C9DT01803D.

ROYAL SOCIETY OF CHEMISTRY

rsc.li/dalton

View Article Online
DOI: 10.1039/C9DT01803D

Synthesis, X-ray structure, physicochemical properties and anticancer activity of *mer* and *fac* Ru(III) triphenylphosphine complexes with a benzothiazole derivative as a co-ligand

Monika Richert,[*a] Mariusz Walczyk,[b] Marcin Janusz Cieślak,[*c] Julia Kaźmierczak-Barańska,[c] Karolina Królewska-Golińska,[c] Grzegorz Wrzeszcz,[b] Tadeusz Muzioł,[b] Stanisław Biniak[b]

[a.] *Faculty of Pharmacy, Collegium Medicum in Bydgoszcz, Nicolaus Copernicus University in Toruń; Jurasza 2; 85-094 Bydgoszcz, Poland;*

E-mail: monika.richert@cm.umk.pl, phone: +48 52 585-38-03, Fax: +48 52 585-38-04

[b.] *Faculty of Chemistry, Nicolaus Copernicus University in Toruń; Gagarina 7, 87-100 Toruń, Poland*

[c.] *Centre of Molecular and Macromolecular Studies, Polish Academy of Sciences, Sienkiewicza 112, 90-363 Lódź, Poland*

Corresponding Authors

View Article Online
DOI: 10.1039/C9DT01803D

*E-mail: monika.richert@cm.umk.pl

*E-mail: marcin@cbmm.lodz.pl – biological part

KEYWORDS**:** *mer*- and *fac*-Ru(III) complexes, benzothiazole derivative, X-ray structures, cyclic voltammetry, cytotoxic effect, log *P*

ABSTRACT

Two mononuclear ruthenium(III) *mer*- and *fac*- isomers of the formula $[RuCl_3(PPh_3)(dmpbt)]$ (where PPh_3 = triphenylphosphine, dmpbt = 2-(3,5-dimethylpyrazoll-yl)benzothiazole) have been synthesised from the reaction of $[RuCl_3(PPh_3)_3]$ with a bidentate ligand – dmpbt. Appropriate reaction conditions allowed to obtain the two isomers separately without separation techniques. X-ray crystallography has determined the crystal and molecular structures of the new complexes. *Mer*-Ru(III) (**1**) crystallised in the monoclinic P2(1)/n, and *fac*-Ru(III) (**2**, **2'**) in the triclinic P–1 space group. The composition of the ruthenium coordination sphere was confirmed and characterised using spectroscopic techniques (FT–IR, UV–vis and EPR), elemental analysis and mass spectrometry (MS–FAB). The structures of the complexes obtained were analysed using X-ray and other spectroscopic methods (IR, UV–vis). The electrochemical properties of the ligand and the complex compound were identified using cyclic voltammetry, determining the potential and charge of faradic processes. Both isomers are redox active and display quasi-reversible metal centered redox processes for the Ru(III)/Ru(II) pair. Moreover, preliminary tests of their biological activity were performed. The cytotoxicity of these compounds has been tested for human lung carcinoma (A549), chronic myelogenous leukemia (K562), human cervix carcinoma (HeLa) cells, acute lymphoblastic leukemia (MOLT-4) and human breast adenocarcinoma cell line (MCF-7) and normal human umbilical vein endothelial cells (HUVEC). The ability to induce apoptosis has

View Article Online
DOI: 10.1039/C9DT01803D

been demonstrated in caspase 3/7 activity assay. In addition, the lipophilicity of both isomers was described by a partition coefficient, log *P*, which values were estimated by the shake-flask method. The interesting and promising preliminary results of the biological and chemical activities of the new octahedral *mer/fac* Ru(III) complexes motivate for further *in vitro* and *in vivo* studies.

INTRODUCTION

The discovery of cisplatin[1] and its anticancer properties significantly influences the development of research concerning metallopharmaceuticals. Despite the large number of different d-electron metals complexes already obtained, it is still necessary to search for new compounds with better therapeutic properties, lower toxicity and greater specificity than cisplatin.[2, 3] Ruthenium(III) complexes seem to be the most attractive and promising prodrug. Ruthenium(III) ions, unlike cisplatin, have a different coordination number and the ligands have other affinities. It caused different kinetics of ligands substitution and redox activity than platinum(II) complexes . The interest in ruthenium complexes as potential anticancer drugs results mainly from three of their properties: a) the rate of ligand exchange comparable with that of platinum(II) compounds and the possibility of controlling this rate through the coordination of ligands with suitably selected properties; b) the wide range of oxidation states (II, III and IV) available under physiological conditions and the possibility of controlling the redox potential and rate of electron transfer by the selection of suitable ligands; and, c) the ability of ruthenium to mimic iron in its ways of binding certain biological molecules like human transferrin.[4-6] The intense study focused on the cytotoxic effects and mechanism of action of ruthenium(III) compounds led to the selection of a few complexes with the most promising properties.

View Article Online
DOI: 10.1039/C9DT01803D

The anticancer activity of imidazolium *trans*-[tetrachloride-bis(1H-imidazole)ruthenate(III)], (Kp418) against murine P388 leukemia and B16 melanoma,[7] as well as the ability to reduce a tumour mass in rats,[8] caused significant research attention of the analogue complexes. These efforts led to identification of two the most promising ruthenium(III) complexes to indazolium *trans*-[tetrachloride-bis(1H-indazole)ruthenate(III)], (KP1019), and imidazolium *trans*-[tetrachloride(1H-imidazole)(S-dimethylsulfoxide)ruthenate(III)] (NAMI-A).[9] NAMI-A, the first ruthenium anticancer compound to be studied on human beings, which demonstrated antimetastatic[10] and anticancer properties. The biological activity studies of NAMI-A proved that it has numerous biological targets as DNA, RNA and proteins.[11] Moreover, the clinical trial of phase I/II showed that NAMI-A with gemcitabine is only moderately tolerated and less active in Non-Small Cell Lung Cancer (NSCLC) patients after first line treatment than gemcitabine alone.[12, 13] Currently, clinical trials include KP1019 (IndH[trans-$RuCl_4(Ind)_2$], where Ind = indazole) and NKP-1339 (Na[trans-$RuCl_4(Ind)_2$]) and ruthenium(II)-arene complexes.[14, 15]. Despite the structural similarities of KP1019 and NAMI-A, they are characterised by different *in vivo* and *in vitro* biological activities. KP1019 is devoid of side effects and causes in cancer cells apoptosis, particularly of colorectal tumours. Anticancer activity studies KP1019 and NKP-1339 have shown their affinity of donor atoms particularly in albumin and transferrin, which are the first potential targets in the transport of ruthenium complexes to tumour cells.[16] The cytotoxic effect is associated with formation of reactive oxygen species (ROS).[17] The group of the ruthenium-arene complexes with PTA (RAPTA) (where PTA = 1,3,5-triaza-7-phosphoadamantane) exhibit excellent antimetastatic and anti-angiogenic activity.[18] Ru(II)–arene organometallic complexes interact with DNA by coordination to the bases and intercalation.[19] In contrast to platinum anticancer drugs, NAMI-A is not very toxic towards a primary tumour, but the main effect of the compound is to

View Article Online
DOI: 10.1039/C9DT01803D

stop tumours from spreading to other parts of a body.[20, 21] NAMI-A is especially active against tumour lung metastases and it is hypothesised that this compound interacts with a target on the tumour cell membrane.[22]

NAMI-A, similarly to KP1019, interacts with DNA, but DNA does not seem to be its primary target. NAMI-A forms intrastrand adducts (Ru-G and Ru-AG) *in vitro,* moreover, both *in vitro* and *in vivo* studies have shown that NAMI-A also binds to the plasma proteins albumin and transferrin.[22, 23] Antimetastatic activity similar to that of NAMI-A was shown by RAPTA-T and various different ruthenium organometallic[14, 24, 25] for which the importance of the ruthenium and ligands arrangement was emphasised.[24, 26, 27] Based on the hypothesis of activation by reduction mechanism, the reduction of NAMI-A was examined in the presence of ascorbic acid used at a physiological concentration. This study has shown the possibility of the reduction of NAMI-A to its corresponding Ru(II) *via* an outer-sphere mechanism.[12]

The discovery of antitumour and antimetastatic activity of ruthenium complexes, especially KP1019 and NAMI-A, caused a considerable increase of the complexes synthesis with similar structures to them.[28] On the other hand, the inspiration came from the investigation of alternative ruthenium(III) complexes with different N,N- and N,S-donor ligands. The choice of the ligand was very often based on its well-known biological activity and an interesting pharmacological profile. Examples of such ligands are pyrazole or benzothiazole and their derivatives, which play an essential role in the design of new drugs. Pyrazole is known as an important and very attractive pharmacophore with diverse therapeutic activities, including: antitumour,[29] antibacterial, anti-inflammatory,[30] anticonvulsant, antidepressant,[31] analgesic and anthelmintic ones.[32] Benzothiazole is still one of the most versatile classes of compounds with antimicrobial activity[33]

View Article Online
DOI: 10.1039/C9DT01803D

and its derivatives are characterised by varied biological activities, namely: antitumour,[34] antitubercular,[35] antimalarial,[36] anticonvulsant,[37] analgesic[38] and anti-inflammatory.[39]

In our work, we have focused on the synthesis of ruthenium(III) complexes with 2-(3,5-dimethylpyrazoll-yl)benzothiazole (dmpbt) as a co-ligand. The rationale for choosing the dmpbt ligand was its successful application in reactions with d-electron metals, such as cobalt,[40] nickel[41] and molybdenum.[42] Complexes of first two metals exhibited substantial cytotoxicity towards HL-60 and NALM-6 leukemia cells and WM-115 melanoma cells, albeit lower as than cisplatin and carboplatin.[40, 41] Moreover, chlorido ligand and phosphine molecule used as ligands in the coordination sphere of ruthenium(III) are intended to hydrolyses facilitate *in vitro* stabilisation of the Ru(II) ions formed by the Ru(III) reduction respectively. The Ru(II) species (such as glutathione in the cell and ascorbic acid in the blood in the human body) is expected to reactive in the hypoxic regions of solid tumour tissues.[43 44] Besides, the structural and spectroscopic characterisation of the new ruthenium(III) complexes, we defined electrochemical properties using the method of cyclovoltammetry to determine the ability of biological activation by a reduction mechanism. Furthermore, obtained compounds showed some biological activities, their lipophilicity was determined. The relationships between analysed properties will give a potential mechanism of anticancer activity and possible further directions for *in vitro* and *in vivo* studies.

MATERIALS

Acetonitrile (MeCN) 99.99% HPLC grade (Sigma-Aldrich), as well as lithium perchlorate ($LiClO_4$, p.a., Acros organics) were used as received. Hydrated ruthenium(III) chloride, triphenylphosphine, buffer PBS saline (pH=7.2), cisplatin and using solvents were purchased from

View Article Online
DOI: 10.1039/C9DT01803D

Aldrich and used as supplied. The 2-(3,5-dimethylpyrazoll-yl)benzothiazole was prepared according to literature procedures.[45]

Synthesis of complex compounds

***mer*-[$RuCl_3(PPh_3)$(dmpbt)] (1)**

Triphenylphosphine (100 mg, 0.384 mmol) was added to a solution of ruthenium(III) chloride (0.096 mmol) in ethanol (10 ml) and hydrochloric acid (37%, 1ml), then the synthesis was carried out according to in the literature.[46] The dmpbt (20 mg, 0.096 mmol) was added to the brown-colored trichlorotriphenylphosphineruthenium(III) ethanolic solution and refluxed for half an hour. The solution became orange. After cooling to room temperature, the product started to precipitate as an orange solid. Crystallisation from mother solution was carried out *via* vapor diffusion technique to obtain a single crystal suitable for X-ray analysis. Diethyl ether was used as a more volatile solvent. After three days yellow orange crystals of *mer*-[$RuCl_3(PPh_3)$(dmpbt)] (**1**) were received. Yield: 0.17 g (75%). Analysis for $RuC_{30}H_{26}N_3PSCl_3$. Calculated (%): C, 51.55; H, 3.75; N, 6.01. Found (%): C, 51.45; H, 3.86; N, 6.16. MS (FAB): m/z = 698.9 [M^+], 399.1 [$RuClPPh_3^+$], 363.0 [$RuPPh_3^+$], 262.1 [PPh_3^+], 229.1 [$dmpbt^+$], 135.0 [benzothiazole], 136.0 [$benzothiazoleH^+$]. UV-vis (acetonitrile, (λ, nm) (ε/dm^3 mol^{-1} cm^{-1}): 257sh (~21400); 275sh (13800); 305 (15600); 388 (3200); 465sh (~640). IR KBr pellet, cm^{-1} and FTIR (CsI pellet, cm^{-1}): 1579 ν(C=N), (pyr, dmpbt-Ru); 1512 ν(C=N), (btz, dmpbt-Ru); 442 ν(Ru-P); 420, 407, 391, 364 ν(Ru-N); 329, 291, 245, 193, 142 ν(Ru-Cl).

***fac*-[$RuCl_3(PPh_3)$(dmpbt)]·H_2O (2)**

The mother solution of the *mer*-[$RuCl_3(PPh_3)$(dmpbt)] (**1**) with orange crystals has remained for the next three weeks. After this time, *mer*-isomer started to converse into dark shine brown needles of the *fac*-[$RuCl_3(PPh_3)$(dmpbt)]·H_2O (**2**). Moreover, the mother solution containing isomers was

View Article Online
DOI: 10.1039/C9DT01803D

left for next three months under the vapor diffusion conditions with diethyl ether. After this time, it was observed that all orange crystals were converted into dark brown needles. Yield: 0.17 g (73%). Analysis for $RuC_{30}H_{28}N_3OPSCl_3$. Calculated (%): C, 50.25; H, 3.94; N, 5.86. Found (%): C, 50.72; H, 4.12; N, 6.16%.

MS (FAB): m/z = 716.5 [M^+], 699.0 [$M^+–H_2O$], 399.0 [$RuClPPh_3^+$], 363.0 [$RuPPh_3^+$], 262.1 [PPh_3^+], 229.1 [$(dmpbt)^+$], 135.0 [benzothiazole], 136.0 [benzothiazoleH$^+$]. UV-vis (acetonitrile, (λ, nm) (ε/dm^3 mol^{-1} cm^{-1}): 257sh, 276sh, 308, 374sh, 476sh, 589. IR KBr pellet, cm^{-1} and FTIR (CsI pellet, cm^{-1}): 1583 ν(C=N), (pyr, dmpbt-Ru); 1508 ν(C=N), (btz, dmpbt-Ru); 448, 439 ν(Ru-P); 414, 407, 391, 369 ν(Ru-N); 329, 291, 247, 194, 143 ν(Ru-Cl); 3451ν(O-H).

***fac*-[$RuCl_3(PPh_3)(dmpbt)]\cdot C_2H_5OH$ (2')**

Triphenylphosphine (100 mg, 0.384 mmol) was added to a solution of ruthenium(III) chloride (0.096 mmol) in ethanol (10 ml) and a mixture of sulfuric acid (95–98%, 1ml) and hydrochloric acid (37%, 1 ml) and then further procedures described in the literature was followed.[46] The dmpbt (20 mg, 0.096 mmol) was added to the brown-coloured trichlorotriphenylphosphineruthenium(III) ethanolic solution and refluxed for about half an hour. The solution became a deep orange colour. Crystallisation was carried out by a vapor diffusion technique. After three weeks, dark shine brown needles of the *fac*-Ru(**2'**) were received, filtered off, washed with petroleum ether, and dried under a vacuum (yield: 0.22 g, 85%). The structure was confirmed by X-ray, mass spectrometry and elemental analyses.

Analysis for $RuC_{32}H_{32}N_3OPSCl_3$. Calculated (%): C, 51.58; H, 4.33; N, 5.64. Found (%): C, 51.60; H, 4.34; N, 5.66%. MS (FAB): m/z = 745.1 [M^+], 699.1 [$M^+–C_2H_5OH$], 399.0 [$RuClPPh_3^+$], 363.0 [$RuPPh_3^+$], 262.1 [PPh_3^+], 229.1 [$(dmpbt)^+$], 135.0 [benzothiazole], 136.0 [benzothiazoleH$^+$]

View Article Online
DOI: 10.1039/C9DT01803D

EXPERIMENTAL METHODS

Magnetic measurements and EPR

Magnetic susceptibility was measured at room temperature by the Faraday method. The magnetic field was calibrated with $Hg[Co(NCS)_4]$.[47] The molar susceptibilities were corrected for diamagnetism using the Pascal's constants[48] (-403×10^{-6} for **1** and -416×10^{-6} cm^3 mol^{-1} for **2**). The effective magnetic moments were calculated from the equation: $\mu_{eff} = 2.828\ (\chi_{Mcorr}\ T)^{½}$.

EPR spectra of the powdered samples were recorded at room temperature with an X band (ca. 9.33 GHz) Radiopan EPR SE/X-2541M spectrometer with a 100 kHz modulation. The microwave frequency was monitored with a frequency meter. The magnetic field was measured with an automatic NMR-type magnetometer.

UV–vis Spectroscopy

Electronic spectra were measured with a Metertech 8001 spectrophotometer in an acetonitrile solution within the 200–1100 nm range.

IR Spectroscopy

IR spectra of the synthesised complexes were obtained using a Perkin-Elmer FTIR Spectrum 2000 spectrometer. Spectra were recorded from 4000 to 400 cm^{-1} (MIR; KBr pellet) and 700 – 30 cm^{-1} (FIR; CsI pellet) at a scan rate of 0.2 cm s^{-1}, and the number of interferograms at a nominal resolution of 4 cm^{-1} was fixed at 25. Before spectrum of a sample was recorded, the background line was obtained arbitrarily and subtracted.

MS–FAB

The MS–FAB data were determined on Finnigan MAT 95 mass spectrometer (NBA, Cs^+ gun operating at 13 keV).

Elemental analyses

View Article Online
DOI: 10.1039/C9DT01803D

Elemental analyses for the obtained complexes were performed on a Vario EL of Elementar Analysensysteme GmbH.

X-ray diffraction data

Hereby, we report structures of two geometrical isomers, *mer*- and *fac*-, obtained in the single synthesis formed as *mer*-[$RuCl_3(PPh_3)$(dmpbt)] (**1**), *fac*-[$RuCl_3(PPh_3)$(dmpbt)]·H_2O (**2**) and *fac*-[$RuCl_3(PPh_3)$(dmpbt)]·C_2H_5OH (**2'**). Suitable crystals were obtained using vapor diffusion technique for all compounds. Diffraction data for the three complexes were collected on Oxford Sapphire with CCD area detector,[49] MoKα radiation λ = 0.71073 Å. All structures were solved by direct methods and refined by full-matrix least-squares techniques on F^2 with SHELXL program.[50] The numerical absorption correction was applied for all crystals (RED171 package of programs, Oxford Diffraction, 2000).[49] Heavy atoms were refined with anisotropic thermal displacement parameters. The positions of hydrogen atoms attached to carbon atoms were assigned at calculated positions. All hydrogen atoms were refined with isotropic thermal displacement parameters fixed to a value of 20% or 50% higher than those of the corresponding carbon atoms. For (**2**), partially occupied water molecules were found, whereas in (**2'**), the ethanol molecule was found in the crystal network. In (**2**), there are no hydrogen atoms attached to water molecules, and in (**2'**), we found partially occupied oxygen atom (0.87/0.13) from ethanol, and in the minor position, the hydrogen atom is missing. All figures were prepared in DIAMOND[51] and ORTEP-3[52] and the interactions were analysed using PLATON.[53] The data for (**1**), and (**2**) are summarized in **Table 1** and data for (**2'**) in **Table S1** (**Supporting Information**). **CCDC 1030325, CCDC 1030304 and CCDC 1826278** contain supplementary crystallographic data for (**1**), (**2**) and (**2'**) respectively. These data can be obtained free of charge from The Cambridge Crystallographic Data Centre *via* **www.ccdc.cam.ac.uk.**

View Article Online
DOI: 10.1039/C9DT01803D

Table 1. Crystal data and structure refinement for (**1**) and (**2**)

Parameters	**(1)**	**(2)**
Empirical formula	$C_{30}H_{26}Cl_3N_3PRuS$	$C_{30}H_{28}Cl_3N_3OPRuS$
Formula weight	698.99	717.00
Temperature [K]	293(2)	293(2)
Wavelength [Å]	0.71073	0.71073
Crystal system, space group	monoclinic, P2(1)/n	Triclinic, P –1
Unit cell dimensions [Å] and [°]	a = 10.6546(3)	a = 8.5500(9)
	b = 17.3387(4)	b = 10.1649(11)
	c = 15.9083(4)	c = 17.926(2)
	β = 97.968(2)	α = 92.169(10)
		β = 97.822(10)
		γ = 99.235(9)
Volume [$Å^3$]	2910.49(12)	1520.6(3)
Z, Calculated density [mg/m^3]	4, 1.595	2, 1.566
Absorption coefficient [mm^{-1}]	0.967	0.930
F(000)	1412	726
Crystal size [mm]	0.42 x 0.13 x 0.08	0.34 x 0.07 x 0.04
Theta range for data collection [°]	2.17 to 26.73	2.03 to 25.02
Limiting indices	$-12 \le h \le 13$	$-9 \le h \le 10$
	$-21 \le k \le 18$	$-12 \le k \le 11$
	$-19 \le l \le 6$	$-21 \le l \le 21$
Reflections collected / unique	11504 / 6134 [R(int) = 0.0468]	8868 / 5358 [R(int) = 0.1162]
Completeness to theta	26.73° 99.3 %	25.02 97.3 %

View Article Online
DOI: 10.1039/C9DT01803D

Absorption correction	Numerical	Numerical
Max. and min. transmission	0.9266 and 0.6869	0.9639 and 0.7434
Refinement method	Full-matrix least-squares on F^2	Full-matrix least-squares on F^2
Data/restraints/parameters	6134 / 0 / 354	5358 / 12 / 372
Goodness-of-fit on F^2	0.967	0.972
Final R indices [I>2sigma(I)]	$R1^a$ = 0.0391, $wR2^b$ = 0.0919	$R1^a$ = 0.0844, $wR2^b$ = 0.1943
R indices (all data)	$R1^a$ = 0.0697, $wR2^b$ = 0.1050	$R1^a$ = 0.1810, $wR2^b$ = 0.2425
Extinction coefficient	----	----
Largest diff. peak and hole [e.Å^{-3}]	1.127 and –0.465	1.842 and –0.756

[a] $R1 = \Sigma || F_0| - | F_c| | / \Sigma | F_0|$ [b] $wR2 = [\Sigma w(F_0^2 - F_c^2)^2 / \Sigma (w(F_0^2)^2)]^{1/2}$

Electrochemical measurements

Cyclic voltammetric measurements were performed using an Autolab (Eco Chemie) modular electrochemical system equipped with a PGSTAT128N potentiostat, controlled by NOVA software and the typical three-electrode electrochemical cell. A platinum microelectrode served as working electrode and another Pt wire and Ag wire were used as counter and reference electrodes, respectively.[54] Cyclic voltammetry measurements were carried out in 0.1 M $LiClO_4$/MeCN base electrolyte solutions using ruthenium(III) chloride, ligands or ruthenium complex as a depolariser. The approximate concentration of the dissolved depolariser was about 50 mM. The potentiometric responses of the working electrode were measured in oxygen-free electrolyte solutions (usually after 24 h). Cyclic voltammetric curves (CVs) were recorded for different sweep amplitudes once electrochemical equilibrium had been established (no changes in repeated CV scans). The data were collected under nitrogen atmosphere in the thermostated system at the room temperature (293 K). The scans start at 0.0 V in anodic direction as indicated by the arrows. From the CVs obtained,

View Article Online
DOI: 10.1039/C9DT01803D

the anodic and cathodic peak potentials were determined with accuracy ±5 mV. All potentials are quoted with respect to employed Ag-wire reference electrode.

Lipophilicity

The lipophilicity of *mer*-Ru(III) (**1**) and *fac*-Ru(III) (**2**) complexes was determined using the shake-flask method.[55, 56] Equal amounts of aqueous phosphate buffered saline and organic n-octanol phases were mixed and saturated for 24 h. Ruthenium complexes and cisplatin were dissolved at a concentration of 0.01 mg/mL in 10 mL of the saturated aqueous phase. An equal volume of PBS was added to n-octanol, and solutions were shaken for 30 minutes, followed by centrifugation (6000 rpm,15 min). After separation, the phases were analysed using UV-vis spectroscopy to determine the amount of the compounds in each phase. The measurements were performed using a SCHIMADZU UV-1800 UV-vis spectrophotometer. The absorption values before and after shaking were compared. The partition coefficient (log *P*) in both phases for each compound was calculated based on the Lambert–Beer Law to determine the log *P* values. The procedures were repeated three times.

Cells and cytotoxicity assay

The HeLa (human cervix carcinoma), K562 (chronic myelogenous leukemia), A549 (human lung carcinoma), MOLT-4 (acute lymphoblastic leukemia) and MCF-7 (human breast adenocarcinoma) cells were cultured in RPMI 1640 medium supplemented with antibiotics and 10% fetal calf serum, in a 5% CO_2 - 95% air atmosphere. $7x10^3$ cells were seeded on each well on 96-well plate (Nunc). Twenty-four hours later, the cells were exposed to the test compounds. Stock solutions (100 mM) of test compounds were freshly prepared in DMSO (dimethylsulfoxide). The final concentrations of the compound (**1**), (**2**), and dmpbt in the cell culture were 1 mM, $1x10^{-1}$ mM, $1x10^{-2}$ mM, $1x10^{-3}$ mM, $1x10^{-4}$ mM and $1x10^{-5}$ mM. The concentration of DMSO in the cell

View Article Online
DOI: 10.1039/C9DT01803D

culture medium was 1%. *Cis*-Pt stock solution of 5 mM was prepared in 0.9% NaCl. The final concentration of the *cis*-Pt in the cell culture was $5x10^{-2}$ mM, $1x10^{-2}$ mM, $2.5x10^{-3}$ mM, $1x10^{-3}$ mM, $2.5x10^{-4}$ mM and $1x10^{-4}$ mM.

Human umbilical vein endothelial cells (HUVEC) were obtained from Life Technologies and cultured in Medium 200 with low serum growth supplement (Life Technologies) according to manufacturer's instructions. $10x10^3$ cells were seeded on each well on 96-well plate (Nunc).

The values of IC_{50} (the concentration of test compound required to reduce the cell survival fraction to 50% of the control) were calculated from dose-response curves and used as a measure of cellular sensitivity to a given treatment.

The cytotoxicity of all compounds was determined by the MTT [3-(4,5-dimethylthiazol-2-yl)-2,5-diphenyltetrazolium bromide; Sigma, St. Louis, MO] assay as described. [57] Briefly, after 48 h of incubation with test compounds, the cells were treated with the MTT reagent for 2 h. MTT-formazan crystals were dissolved in lysis buffer (20% SDS and 50% DMF, pH 4.7) and absorbance was read at 570 and 650 nm on an ELISA-PLATE READER (FLUOstar Omega). As a control (100% viability), we used cells grown in the presence of only vehicle (1% DMSO).

Caspase-3/7 assay

$20x10^3$ of HeLa cells were seeded on each well of 96-well plate in RPMI 1640 medium supplemented with 10% fetal calf serum and antibiotics. The cells were grown for 24 h at 37°C and 5% CO_2. The test compounds were dissolved in DMSO (except for *cis*-Pt which was dissolved in 0.9% NaCl) and added to the cell culture. Untreated cells or cells treated with 1% DMSO served as a negative control, while cells incubated with staurosporine (a potent inducer of apoptosis) were used as a positive control. The cells were exposed to the test compounds for 18 h at 37°C and 5% CO_2. Subsequently, the activity of caspase 3 and 7 was measured by Apo-ONE® Homogeneous

View Article Online
DOI: 10.1039/C9DT01803D

Caspase-3/7 Assay (Promega, Madison, WI, USA) according to the manufacturer's instructions. Briefly, the cells were lysed and incubated for 1.5 h with profluorescent substrate for caspase 3 and 7. Next, the fluorescence was read at an excitation wavelength of 485 nm and emission of 520 nm with FLUOStar Omega (BMG-Labtech, Germany) plate reader.

RESULTS AND DISCUSSION

Synthesis

One of the ligands used in the described synthesis was bidentate chelating 2-(3,5-dimethylpyrazoll-yl)benzothiazole. Dmpbt with two non-equivalent nitrogen atoms, chlorido ligand and triphenylphosphine, after coordinating to the ruthenium ion formed two geometric stereoisomers, *mer* and *fac* of the $[RuCl_3(PPh_3)(dmpbt)]$ formula. The dmpbt ligand was prepared by the described method[45] and characterized by elemental analysis, IR (**Supporting Information, Figure S1**) and ^1H NMR data (**Supporting Information, Figure S2**).

Mer-$[RuCl_3(PPh_3)(dmpbt)]$ (**1**) complex was synthesised by the reaction of $[RuCl_3(PPh_3)_3]$ and dmpbt in the M:L=1:1 molar ratio, (where M – metal, L – ligand) in refluxing with ethanolic solution. $[RuCl_3(PPh_3)_3]$ was prepared according to the literature methods.[46] The *fac*-Ru(III) (**2**) isomer was obtained in the isomerisation reaction of (**1**) or in similar reaction as a *mer*, but with the use of 1:1 (v/v) sulphuric and hydrochloric acids mixture. According to the literature, [58, 59] synthesis of ruthenium complex isomers kinetically favours a *mer* isomer as the first product. The electronic *trans* effect explains the thermal conversion of a *mer* into a *fac* isomer. Another way for this conversion is photochemical isomerisation. For example *fac*-$[RuCl_3(NO)(dppb)]$, (dppb = 1,4-bis(diphenylphosphino)butane) was obtained from *mer*, which was refluxed for 4 h under argon.[60] However, the same authors have shown that *fac*-$[RuCl_3(NO)(P–P)]$ isomers can be obtained from

View Article Online
DOI: 10.1039/C9DT01803D

a similar reaction but with different diphosphines ((P–P) = $R_2P(CH_2)_nPR_2$ (n = 1–3) and $R_2P(CH_2)POR_2$, PR_2–CH=CH–PR_2, where R = C_6H_5 and $(C_6H_{11})_2P$–$(CH_2)_2$–$P(C_6H_{11})_2$), which has been explained by steric reasons. The isomer *mer*-[$RuCl_3(NO)$(P–P)] was received from the corresponding *fac*-isomer by using white light.[61] Another example of photochemical isomerisation is the conversion of *fac*-[$RuCl_3(NO)$(P–N)] (P–N = *o*-[(*N,N*-dimethylamino)phenyl]diphenylphosphine) to *mer*-[$RuCl_3(NO)$(P–N)].[62] One of the main problems of the *mer* and *fac* isomers synthesis is their separation. Fletcher and co-workers[63] carried out the separation of both Ru(II) complexes isomers using a stepwise templated synthesis or through the separation by preparative plate chromatography.[59, 64] It is known in the literature that the formation of the *mer* isomer more likely than *fac*. The last studies have shown that the change in the solvent and reaction conditions can lead to the pure *fac* isomer,[64] which was confirmed in our studies. The first synthesis product, the *mer*-Ru(III) (**1**) isomer, was formed as orange crystals (in the mother solution under conditions of the diffusion process). The *mer* isomer slowly converted to *fac* as dark shiny brown needle crystals. The observed colour change was assigned to structural conversion. It can be a comfortable and straightforward method for the detection of structural transformation.[65, 66] Whereas, pure *fac*-Ru(III) (**2'**) isomer was obtained from a similar reaction as *mer*-Ru(III) (**1**) but with the use of mixture HCl and H_2SO_4. The structural change of the *mer* to *fac* isomer is probably caused by structural transformations–"single crystal-to-single crystal" (SCSC), which is often difficult.[65, 66] Among many external factors (*e.g.* temperature, pressure, irradiation, solvent, concentration), the solvent probably plays a significant role in the *mer*-Ru(III) (**1**) into *fac*-Ru(III) (**2**) transformation.[66, 67] Change of the *fac*-Ru(**2'**) synthesis conditions (use of 1:1 (v/v) sulphuric and hydrochloric acids mixture) probably caused formation of the *fac*-isomer as more thermodynamically stable product (**2'**) and the presence of the ethanol

View Article Online
DOI: 10.1039/C9DT01803D

molecule (guest molecule) in the crystal lattice of (**2'**). The ability to control the reaction by maintaining appropriate conditions gives us the selectivity and purity of the products reactions and is undoubtedly a significant advantage.

The differences in the cell parameters and symmetry crystals of the *fac* isomers (**2** and **2'**) do not influence the behaviour in solution (UV-vis analysis), which is essential for biological studies.

Analysis of IR spectra

Spectra analysis was limited mainly to the 160–1600 cm^{-1} range, in which the presence of benzothiazole, pyrazole, phosphine groups and their connection with metal are studied. The presence of a water molecule was confirmed in the region of 3000–1600 cm^{-1} for the *fac*-Ru(III) (**2**). Characteristic IR frequency bands of the *mer*-Ru(III) (**1**), and *fac*-Ru(III) (**2**) complexes and their assignments are given in **Table S2 (Supporting Information).**

Comparison of the infrared spectra of the 2-(3,5-dimethylpyrazoll-yl)benzothiazole, and its complexes indicated the coordination of the ligand to the metal through tertiary nitrogens on the benzothiazole and pyrazole group. It is confirmed by the presence of ν(C=N) (benzothiazole) vibrations at 1579 cm^{-1}, 1583 cm^{-1} and ν(C=N)(pyrazole) at 1512 cm^{-1}, 1508 cm^{-1} for (**1**) and (**2**) isomers respectively. Additional founded bands in the 360 to 420 cm^{-1} range of the Ru–N bond. According to literature data,[68] bands of ν(Ru–N) appear in the 370–380 cm^{-1} and 450–475 cm^{-1} range. The letter region is a very close range (440–455 cm^{-1}) of the bands Ru–P.[69] The ν(Ru–P) bond vibrations in spectra of (**1**) and (**2**) complexes were found at 442 and 448 cm^{-1}, respectively. Frequency positions of the ν(Ru–N) infrared bands located in the lower frequency and lower intensity than ν(Ru–P). It is probably caused by the high electron density on the metal atom of the Ru–P bond. The other characteristic bands related to triphenylphosphine (around 1432, 1089, 741, 695, 519 cm^{-1}) are also noticeable in both isomers spectra and confirm the presence of PPh_3 in the

View Article Online
DOI: 10.1039/C9DT01803D

ruthenium coordination sphere.[69-71] The presence chloride (σ/π donor ligand), decreases the electron density on the ruthenium centre and, therefore, the ν(Ru–Cl) vibrations appeared in the region of 130–350 cm^{-1}, the lowest frequencies of the metal-ligand bonds in (**1**), (**2**) complexes.[71] Moreover, the presence of water molecules in the crystal structure of the (**2**) complex is confirmed by the broad O–H stretching band at 3451 cm^{-1} and at 1741 cm^{-1} [72], confirmed.

Magnetism and EPR

At room temperature (295 K), the *mer*-[$RuCl_3(PPh_3)$(dmpbt)] (**1**) and *fac*-[$RuCl_3(PPh_3)$(dmpbt)]·H_2O (**2**) complexes have a magnetic moment equal to 1.99 and 2.02 B.M., respectively, which are typical of one unpaired electron systems, and the values are consistent with low-spin d^5 ruthenium(III) in an octahedral environment. The μ_{eff} are somewhat higher than the expected spin-only value of 1.73 B.M. The orbitally degenerate $^2T_{2g}$ (O_h) ground state is split due to spin-orbit coupling and low symmetry ligand field effects.

The EPR spectrum of (**1**) in the solid state (**Figure S3**) exhibited three distinct resonances characteristic of a rhombic symmetry S = ½ spin system with $g_1 = 2.48$, $g_2 = 2.26$, and $g_3 = 1.77$. The EPR spectrum of (**2**) exhibited two distinct resonances characteristic of an axial symmetry S = ½ spin system with $g_\perp = 2.27$ and $g_\parallel = 1.82$. However, because of its poorer quality, the small rhombic component cannot be excluded. The difference between the EPR spectra of (**1**) and (**2**) isomers is similar to that observed in *mer*- and *fac*-[$RuCl_3(As(Ph_3)_3$], which show rhombic and axial spectra, respectively. [73] Hence, the EPR data are characteristic of ruthenium(III) present in a distorted octahedral ligand environment as observed in the crystal structure of both isomers with larger deformation in the *mer* isomer.

UV–vis

View Article Online
DOI: 10.1039/C9DT01803D

The electronic spectra of *mer*-[$RuCl_3(PPh_3)$(dmpbt)] (**1**) and *fac*-[$RuCl_3(PPh_3)$(dmpbt)]·H_2O (**2**) isomers and ligands were recorded in an acetonitrile solution. The *mer*-[$RuCl_3(PPh_3)$(dmpbt)] isomer exhibits intense high-energy absorption overlapping bands in the range from 200 to 280 nm with shoulders at 257 and 275 nm, weaker absorptions at 305 and 388 nm with a low-energy shoulder at 465 nm (molar coefficients are ~21400, ~13800, 15600, 3200, and ~640 $dm^3\ mol^{-1}\ cm^{-1}$, respectively). The (**1**) isomer shows strong high-energy absorptions in the range from 200 to 290 nm with shoulders at 257 and 276 nm (spectra were collected for a saturated solution and molar coefficients are not calculated.). Weaker bands with peak maxima at 308 and 589 nm with shoulders at 374 and 476 nm are also observed. For both isomers the absorptions in the ultraviolet region below 350 nm are very similar and are attributed to the transitions within the ligand orbitals ($\pi\rightarrow\pi^*$ and $n\rightarrow\pi^*$), of the PPh_3 and dmpbt ligands. The absorptions observed in the region of 388–374 nm are probably due to ligand-metal charge transfer transitions taking place from the filled ligand orbitals to the singly-occupied ruthenium orbital. The low energy absorptions in the region of 465–589 nm are attributed to dipole-forbidden *d–d* transitions of the ruthenium(III) ion in a distorted octahedral environment.[74]

As expected, the electronic spectrum of *fac*-[$RuCl_3(PPh_3)$(dmpbt)]·C_2H_5OH (**2'**) recorded in acetonitrile solution is identical, within experimental error, to the spectrum of (**2)**.

X-ray

Hereby, we report the structures of the two geometrical isomers formulated as *mer*-[$RuCl_3(PPh_3)$(dmpbt)] (**1**) and *fac*-[$RuCl_3(PPh_3)$(dmpbt)]·H_2O (**2**). Their corresponding selected bond lengths and angles are given in **Table 2**.

The *fac* isomer was also obtained as *fac*-[$RuCl_3(PPh_3)$(dmpbt)]·C_2H_5OH (**2'**), structural data for which, description and short comparison with (**2**) are given in the Supporting Information (**Table**

View Article Online
DOI: 10.1039/C9DT01803D

S3, Table S4, and Figure S4). The minor product, *mer*-[$RuCl_3(PPh_3)$(dmpbt)] (**1**), crystallised in the monoclinic $P2_1/n$ space group with all atoms in general positions and the whole molecule given by the formulae in the asymmetric unit (**Figure 1**). The crystal date and refinement for **(1)** and **(2)** are presented in **Table 1.**

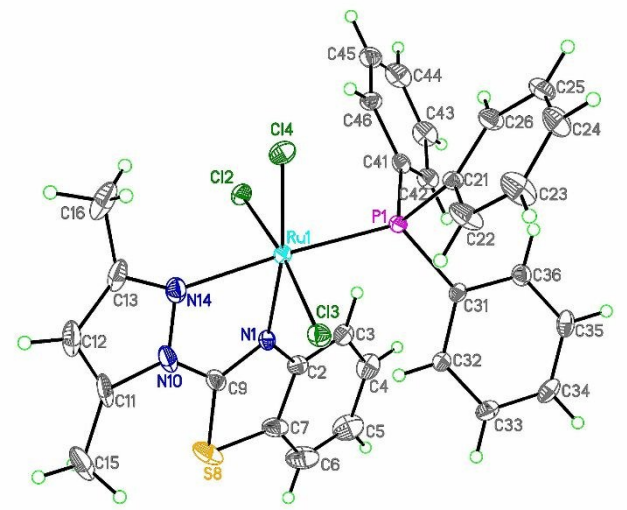

Fig. 1 Molecule of *mer*-[$RuCl_3(PPh_3)$(dmpbt)] (**1**) with the numbering scheme and the thermal ellipsoids at 20% probability.

Table 2. Selected bonds lengths (Å) and angles (º) for (**1**) and (**2**)

Complex	**(1)**		**(2)**	
Distances (Å)				
	Ru1–N1	2.105(3)	Ru1–N14	2.083(9)
	Ru1–N14	2.172(3)	Ru1–N1	2.118(8)
	Ru1–Cl4	2.3247(10)	Ru1–Cl2	2.326(3)
	Ru1–P1	2.3368(9)	Ru1–Cl3	2.326(3)
	Ru1–Cl2	2.3413(9)	Ru1–P1	2.374(4)

View Article Online
DOI: 10.1039/C9DT01803D

	Ru1–Cl3	2.3458(9)	Ru1–Cl1	2.438(4)
Angles (º)	N1–Ru1–N14	75.78(13)	N14–Ru1–N1	77.5(4)
	N1–Ru1–Cl4	171.39(9)	N14–Ru1–Cl2	172.3(3)
	N14–Ru1–Cl4	95.90(10)	N1–Ru1–Cl2	95.6(2)
	N1–Ru1–P1	103.82(9)	N14–Ru1–Cl3	96.5(3)
	N14–Ru1–P1	174.92(9)	N1–Ru1–Cl3	173.9(2)
	Cl4–Ru1–P1	84.67(4)	Cl2–Ru1–Cl3	90.39(12)
	N1–Ru1–Cl2	84.56(8)	N14–Ru1–P1	91.3(3)
	N14–Ru1–Cl2	90.93(9)	N1–Ru1–P1	93.1(3)
	Cl4–Ru1–Cl2	93.47(4)	Cl2–Ru1–P1	92.60(13)
	P1–Ru1–Cl2	94.07(3)	Cl3–Ru1–P1	86.09(12)
	N1–Ru1–Cl3	87.92(8)	N14–Ru1–Cl1	85.3(3)
	N14–Ru1–Cl3	84.04(9)	N1–Ru1–Cl1	89.1(3)
	Cl4–Ru1–Cl3	93.48(4)	Cl2–Ru1–Cl1	91.06(13)
	P1–Ru1–Cl3	90.90(3)	Cl3–Ru1–Cl1	91.30(12)
	Cl2–Ru1–Cl3	171.80(3)	P1–Ru1–Cl1	175.51(13)

In (**1**) the ruthenium coordination sphere adopts a slightly distorted octahedral environment. It consists of two nitrogen atoms from the organic ligand, a phosphorous atom from triphenylphosphine and three chloride ligand occupying *mer* positions. The N14 pyrazole atom is positioned *trans* to the phosphorous atom, whereas the N1 atom is positioned *trans* to the Cl4 chloride anion. The angles between these *trans* positioned atoms are close to 180º and range from 171.39(9) to 174.92(9)º. The *cis* positioned atoms form angles ranging from 75.78(13) to 103.82(9)º. Distances in the coordination sphere fall into two ranges: shorter bonds were found for

View Article Online
DOI: 10.1039/C9DT01803D

nitrogen atoms [2.105(3) and 2.172(3) Å] and longer for phosphorous [2.3368(9) Å] and chlorine atoms [from 2.3247(10) to 2.3458(9) Å]. All rings remain flat within an rms deviation of 0.028 Å observed for the N1 benzothiazole ring. The chelate ring is the only folded ring with an rms of 0.118 Å. The C2 and N1 rings form the smallest dihedral angle of 5.3(2)º. However, four fused rings (C2, N1, chelate and N10) are relatively coplanar with the biggest angle being 15.51(18)º. The three phenyl rings are twisted and the angles between them are 52.13(19), 70.6(2) and 83.0(2)º. This mutual orientation of these phenyl rings results from intramolecular C–H…Cl hydrogen bonds and steric hindrance. Additionally, this conformation is influenced by numerous intramolecular interactions formed between aromatic rings, mainly involving the C31 phenyl group. In the packing the shortest two Ru(III)–Ru(III) contacts (7.436 and 8.367 Å) occur for zigzags running along the *a* axis (**Figure 2**).

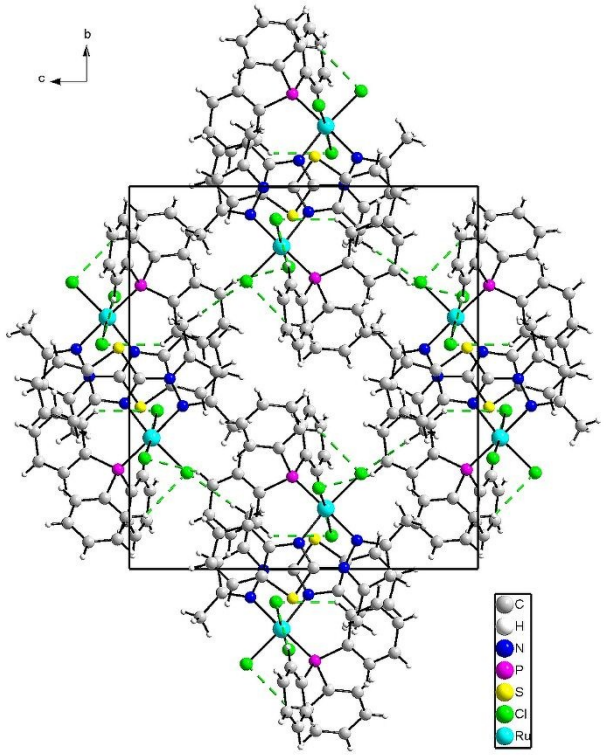

Fig. 2 Packing of (**1**) along a axis with marked C–H…Cl hydrogen bonds (dashed green lines).

View Article Online
DOI: 10.1039/C9DT01803D

Weak interactions usually maintain the crystal network. There are only two intermolecular hydrogen bonds: C15–H15B…Cl4(1/2–x, –1/2+y, 1/2–z) and C35–H35…Cl2(–1/2+x, 1/2–y, 1/2+z) formed with molecules from adjacent zigzags translated along the *c* axis. Apart from these hydrogen bonds we found numerous π–π interactions. The closest ruthenium ions can interact *via* π–π interactions formed by the significantly inclined C31 phenyl ring (PPh_3) and rings from dmpbt. In contrast, the interactions between molecules related by (1–x, –y, 1–z) are assured by stacking interactions formed by organic ligands. Interactions between adjacent zigzags are maintained by π–π interactions between edge-to-face or edge-to-edge oriented rings.

Fac-[$RuCl_3(PPh_3)$(dmpbt)]·H_2O (**2**), crystallised in the triclinic P–1 space group with all atoms in general positions and the whole molecule is given by the formulae in the asymmetric unit (**Figure 3**). The refinement details are presented in **Table 1.**

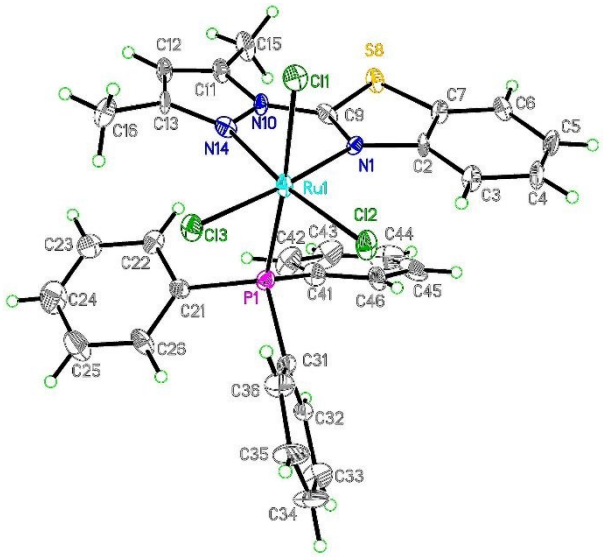

Fig. 3 Molecule of (**2**) with the numbering scheme and the thermal ellipsoids at 20% probability. O51 and O52 partially occupied crystallization water molecules are omitted for clarity.

View Article Online
DOI: 10.1039/C9DT01803D

In (**2**) the ruthenium coordination sphere adopts a slightly distorted octahedral environment. It consists of two nitrogen atoms from the organic ligand, a phosphorous atom from triphenylphosphine and three chlorido ligands occupying *fac* positions. Cl1, Cl2 and Cl3 chlorine atoms are *trans* positioned to P1, N14 and N1 atoms, respectively. The angles between the *trans* positioned atoms range from 172.3(3) to 175.51(13)º. The *cis* positioned atoms form angles ranging from 77.5(4) to 96.5(3)º. The smallest value is observed for the chelate ring. Distances in the coordination sphere fall into two ranges: shorter bonds were found for nitrogen atoms [2.083(9) and 2.118(8) Å] and longer for phosphorous [2.374(4) Å] and chlorine atoms [from 2.326(3) to 2.438(4) Å]. The benzothiazole ligand is flat within an rms deviation of 0.085 Å and even the chelate ring remains flat within rms deviation of 0.049 Å. The C2 and chelate rings form the smallest dihedral angle of 1.09º. The whole ligand remains planar and the biggest angle between its rings is 12.52º for N10 and S8 rings. Three phenyl rings from triphenylphosphine are planar within 0.012 Å. They are twisted and the angles between them are 49.98, 73.16 and 89.27º. The smallest value is found for C21 and C41 phenyl rings, whereas C21 and C31 rings are oriented perpendicularly. Mutual orientation of the phenyl rings results from intramolecular C–H…Cl hydrogen bonds and steric hindrance as well as numerous intramolecular interactions formed between aromatic rings, involving mainly the C41 phenyl group. In the packing we observe *ab* layers composed of zigzags running along the *b* axis. Ru–Ru distances in the zigzag are 8.057 and 8.705 Å, whereas the closest Ru–Ru distance between zigzags is 8.550 Å (**Figure 4**).

View Article Online
DOI: 10.1039/C9DT01803D

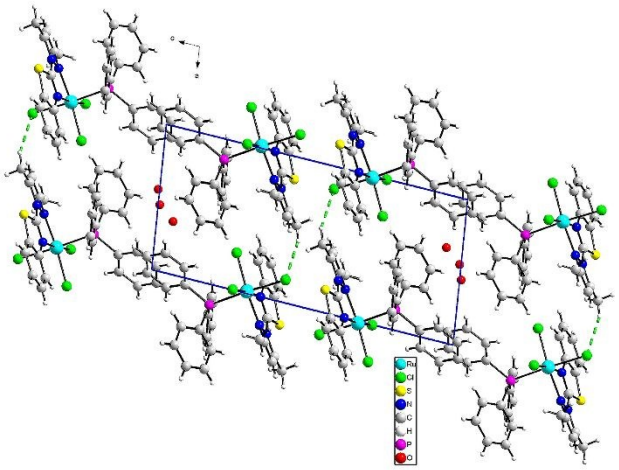

Fig. 4 Packing of (**2**) along b axis with marked intermolecular C–H…Cl hydrogen bonds (dashed green lines).

The separation between ruthenium ions coming from different layers is much longer and exceeds 11 Å. In the zigzag molecules are connected by numerous π–π interactions, mainly by benzothiazole moieties (S8 and C2 rings) which are almost coplanar forming stacking interactions. They seem to be strong due to the mutual orientation of the rings and its small separation (in a consequence the slippage is also very small). Additionally, the moieties in the chain are connected with the C2 ring *via* C15–H15…π interactions. The layer is formed by the only intermolecular C15–H15A…Cl1[–1+x, y, z] hydrogen bond and π–π interactions between almost perpendicularly oriented C21 and C31 phenyl rings from the triphenylphosphine molecule. Interactions between adjacent layers are assured by π–π interactions between two edge-to-edge oriented C21 phenyl rings and stacking interactions between C31 phenyl rings. In the latter case these rings form a zipper running along the *b* axis. Water molecules are loosely packed in the space between adjacent layers. There are no hydrogen atoms belonging to the O51 and O52 crystallisation water molecules. However, it seems they are not involved in essential network interactions.

View Article Online
DOI: 10.1039/C9DT01803D

Both isomers reveal similar geometry. However, careful inspection of **Table 1** shows that there are significant differences, such as inversion of Ru–N distances. In the *mer* form the Ru–N14 (pyrazole) bond is much longer than the Ru–N1band in this complex as well as much shorter than the analogous bond in the *fac* isomer. The difference between the Ru–N14 bonds is 0.09 Å. In the *fac*-Ru(III) (**2**), N14 is positioned *trans* to a chlorine atom, whereas in the *mer*-Ru(III) (**1**) isomer it is positioned *trans* to phosphorous. The difference between the Ru–N1 bonds is much smaller (0.013 Å) but in both structures these atoms are *trans* to chlorine atoms. In the *mer* (**1**) isomer we observe Ru–Cl/P bonds ranging from 2.32 to 2.34, whereas in the *fac* (**2**) form two Ru–Cl distances are 2.32 Å, but the third chlorine (Cl1) forms a very long bond (2.44 Å). This atom is positioned *trans* to phosphorous. It results in mutual elongation of the Ru–Cl1 and Ru–P1 bonds, because the latter was found to be 2.37 Å, revealing elongation by 0.04 Å according to the *mer* isomer. It might be related to lower the lipophilicity of the *fac* (**2**) isomer than *mer*-isomer (expressed as log *P*). We observed better solubility of complex (**2**) and can expect faster ligand substitution in the coordination sphere. We hypothesise that longer Ru–Cl is more susceptible to splitting and this might result from the *trans* effect of the phosphorous ligand (if the influence of the *trans* ligands is the same as in four-coordinated square planar complexes). The chloride substitution would be much slower for the *mer* (**1**) isomer because the trans effect expected for phosphorous is stronger. Hence, dissociation of such a ligand is more difficult because cleavage of one bond is not enough, the second bond still exists and the broken bond can be reformed. We found also that the *fac* (**2**) isomer shows a slightly smaller surface (507.75 *vs.* 523.97 Å) and asphericity (a measure of anisotropy, 0.025 *vs.* 0.037), whereas globularity is bigger (0.766 *vs.* 0.741). These parameters seem to confirm the lower lipophilicity of the *fac* (**2**) isomer. The valence angles also show significant differences, especially for atoms in the *cis* positions. In the *fac* isomer, they range from

View Article Online
DOI: 10.1039/C9DT01803D

77.5(4) to 96.5(3)º and in the *mer* from 75.78(13) to 103.82(9)º. In the latter case the biggest value was observed for N1–Ru1–P1. These differences might be ascribed to two factors: the *trans* effects of different donor atoms and steric hindrance which should be bigger in case of *fac* (**2**) isomer because two huge ligands (triphenylphosphine and dmpbt) – are close to each other – phosphorous is *cis* to both nitrogen, whereas in the *mer* form it is *trans* to N14 and *cis* to N1 atoms. We can observe this effect in the mutual orientation of rings coming from both organic ligands, whereas the angles between rings from the same ligand are similar in both structures. The dihedral angles between the sulphur ring and phenyl rings of triphenylphosphine are 25.89, 27.18 and 71.48º for the *fac* (**2**) structure and 36.33, 50.47 and 61.7º for the *mer* (**1**)isomer.

Electrochemical behaviour

It is commonly believed that ruthenium(III) complexes may be active as prodrugs, which are activated by reduction *in vivo* to the usually less inert Ru(II) species than ruthenium(III) forms.[4, 75] Therefore, the reduction of ruthenium(III) to ruthenium(II) is preferable in a tumour where there is a relatively low electrochemical potential and low pH as well as less oxygenation than in normal tissue.[75] Electrochemical properties of ruthenium compounds were defined using a cyclic voltammetry to determine the possibility of the "activation by reduction" mechanism. The half-wave potentials ($E_{1/2}$) *vs*. Ag-wire reference electrode of the ferrocene (Fc)/ferrocenium (Fc^+) couple in the investigated organic solvent media have been obtained. Ferrocene undergoes a reversible one-electron transfer process in the investigated solvent media.[76] The half-wave potential ($E_{1/2}$) of the ferrocene (Fc)/ferrocenium (Fc^+) couple is 0.25 V *vs*. Ag-wire in the 0.1 M $LiClO_4$/MeCN base electrolyte solutions.

View Article Online
DOI: 10.1039/C9DT01803D

The electrochemical properties of the ruthenium(III) chloride, ligands or ruthenium complex were investigated by cyclic voltammetry in an acetonitrile solution at a scan rate of 2 mV s^{-1} using 0.1 M $LiClO_4$ as the supporting electrolyte. The quasi-reversible character of the electrode reaction is characteristic of the Ru(III)/Ru(II) and Ru(IV)/Ru(III) couples. The anodic (E_a) and cathodic (E_c) potentials (V *vs* Ag-wire) as well as the anodic/cathodic peaks currents and charge ($i_{a/c}$ and $Q_{a/c}$, respectively) are listed in **Table 3**. Additionally, the half-wave potentials characteristic ($E_{1/2}$) and anodic/cathodic peak current relation (abs(i_a/i_c)) of all of the redox pairs were calculated and are also presented in **Table 3.**

Table 3. Selected chemical properties of the ligands and complexes (CV measurements)

compound	E_a, V	i_a, A g^{-1}	Q_a, C	E_c, V	i_c, A g^{-1}	Q_c, C	$E_{1/2}$, V	ΔE, V	i_a/i_c
$RuCl_3$	0.063	2.62E-05	1.87E-06	–0.107	–5.45E-05	2.63E-06	–0.02	–0.17	2.08
PPh_3	-	-	-	-	-	-	-	-	-
dmpbt	0.066	9.68E-07	6.27E-08	–0.183	–4.24E-07	2.59E-08	–0.06	–0.25	2.28
***mer* (1)**	0.049	5.71E-06	7.05E-07	–0.127	–1.20E-05	5.07E-07	–0.04	–0.18	0.47
	0.476	2.91E-06	5.48E-07	0.391	–3.01E-06	7.09E-07	0.43	–0.09	0.97
***fac* (2)**	0.054	2.02E-05	2.27E-06	–0.142	–3.46E-05	1.76E-06	–0.04	–0.20	0.58

The electrochemistry of ligands both PPh_3 and dmpbt undergo no or little activity in the solvent limit (dashed lines in **Figure 5**).

View Article Online
DOI: 10.1039/C9DT01803D

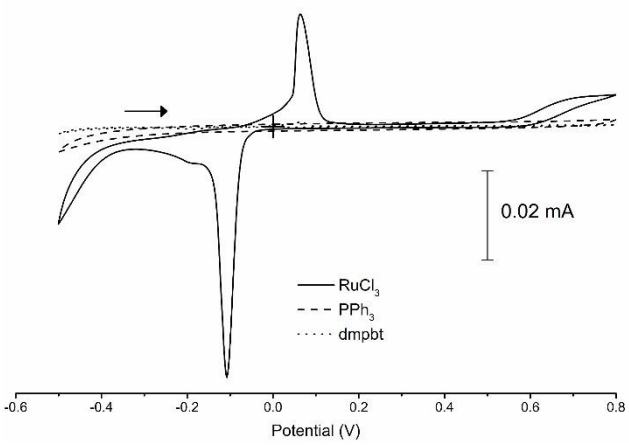

Fig. 5 Cyclic voltammogram of $RuCl_3$ and PPh_3 and dmpbt ligands in 0.2 M *n*-Bu_4NPF_6 in acetonitrile at a platinum working electrode (scan rate 0.2 V s^{-1}).

***mer*-[$RuCl_3(PPh_3)$(dmpbt)] (1)**

The electrochemical data are listed in **Table 3**. **Figure 6** shows a typical cyclic voltammetry curve recorded in the presence of the (**1**) complex, where two redox couples exist in the potential range from –0.6 to 0.8 V *vs*. Ag wire. The anodic peak at approximately 0.05 V and cathodic peak at a potential of approximately –0.13 V correspond to the oxidation of Ru(II) to Ru(III) and the reduction of Ru(III) to Ru(II), respectively. This couple represents a quasi-reversible with an anodic to cathodic peak separation (equal to 0.18 V). The second redox couple is situated in a more positive potential range, and is associated with the reduction and oxidation of the Ru(IV)/Ru(III) couple (cathodic peak 0.39 V and anodic peak 0.48 V). The reactions of these couples are reversible. However, in the case of the first scan, only the second redox couple was observed, namely a Ru(IV)/Ru(III) pair, and a poorly formed cathodic peak (E_c = –0.15 V) of the reduction of Ru(III) to Ru(II).[77]

View Article Online
DOI: 10.1039/C9DT01803D

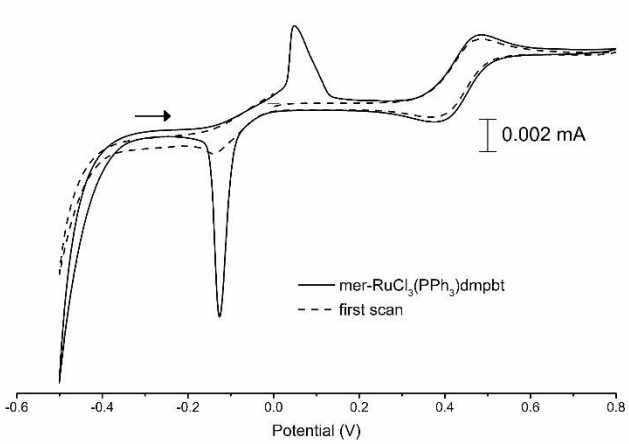

Fig. 6 Cyclic voltammogram of *mer*-[$RuCl_3(PPh_3)$(dmpbt)] (**1**) in 0.2 M *n*-Bu_4NPF_6 in acetonitrile at a platinum working electrode (scan rate 0.2 V s^{-1}).

fac-[$RuCl_3(PPh_3)$(dmpbt)]·H_2O (2)

Another series of CV curves was obtained for the (**2**) complex, where only one a quasi-reversible couple in the potential range from –0.6 to 0.8 V *vs*. Ag wire was observed, with an anodic to cathodic peak separation of 0.20 V (**Figure 7**). In this case, these peaks are attributed to the oxidation of Ru(II) to Ru(III) (E_a ~ 0.05 V *vs*. Ag-wire) and the reduction of Ru(III) to Ru(II) (E_c ~ –0.14 V *vs*. Ag-wire). Just as in the above case, in the first scan a well-formed cathodic peak (E_c = –0.13 V) of the reduction of Ru(III) to Ru(II) is observed.

The cyclic voltammetric investigation of the *fac*-[$RuCl_3(PPh_3)$(dmpbt)] shows that the +III state of ruthenium is stable in the *fac*-(N–N–P–Cl_3) coordination sphere. However, in the case of the *mer*-(N–N–P–Cl_3) coordination sphere the less stable complex was observed, because it was easier to oxidise to ruthenium(IV).

View Article Online
DOI: 10.1039/C9DT01803D

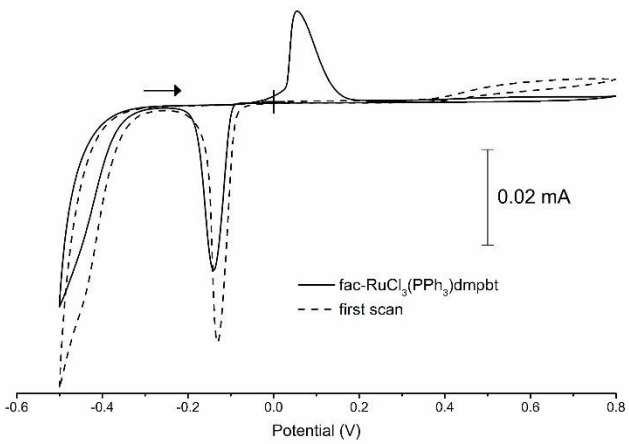

Fig. 7 Cyclic voltammogram of *fac*-[$RuCl_3(PPh_3)$(dmpbt)] (**2**) in 0.2 M *n*-Bu_4NPF_6 in acetonitrile at a platinum working electrode (scan rate 0.2 V s^{-1}).

According to the literature,[78] the reduction potential of proliferating cells is about –0.24 V *vs*. NHE (NHE – normal hydrogen electrode) which corresponds to a value –0.6 V *vs*. Ag-wire in reference to our conditions. Moreover, this potential is 100 mV lower inside cancer cells. The measured Ru(III)/Ru(II) and Ru(IV)/Ru(III) pair potentials indicate that the complexes should have a bioavailable reduction potential.

The physiologically available redox potential is in the range of around –0.4 V to +0.8 V *vs*. NHE. Taking into account the physiological species (NADPH as the reductant[79] and dioxygen as the oxidant) this potential suggests a possible activation by the reduction process of the ruthenium(III) isomers in the biological environment. However, the role of Ru(IV) as a metallodrug has not yet been investigated.

Lipophilicity

Lipophilicity is an important feature characteristic of a substance with potential biological activity. This physicochemical property provides information about the diffusion of drugs through

View Article Online
DOI: 10.1039/C9DT01803D

cell membranes and characterises the potential *in vivo* pharmacokinetic (absorption, distribution, metabolism processes).[80]

The lipophilicity (the partition coefficient, log *P*) can be defined as the ratio of the unionised compound concentration at equilibrium between the organic (*n*-octanol) and aqueous phases (water, buffer saline).

The log *P* value of –2.12 ± 0.04 obtained for *cis*-Pt is within the range reported in the literature.[81] The log *P* of the *mer*-Ru(III) (**1**) and *fac*-Ru(III) (**2**) values were equal to 3.31 ± 0.05 and 2.95 ± 0.05 for (**1**) and (**2**), respectively. According to the literature,[82, 83] the optimal log *P* for drug transport are in the range of 2.0 to 3.5. Moderately lipophilic molecules tend to exhibit the best pharmacokinetic properties.[84] Moreover, log $P > 0$ suggests that the compounds may accumulate specifically in mitochondria and the endoplasmic reticulum,[85] but this requires detailed studies.

The *fac*-isomer (**2**) has a lower lipophilicity than *mer*-isomer (**1**), probably due to the differences in the distorted octahedral geometry for the Ru(III) centre environment which can result in a higher dipole moment for the *fac*-(**2**) isomer. The relationship between structure of complexes and lipophilicity may suggest their different biological activity, *e.g.* cytotoxic.

Cells and cytotoxicity assay

In the screening studies four compounds were tested for their cytotoxic properties in K562, A549, HeLa, MOLT-4, MCF-7 cells, and HUVEC as a non-cancerous cells. Cells treated with 1% DMSO (vehicle) served as the control (100% viability in the MTT assay). Based on the viability of cells measured at different concentrations of test compounds, the IC_{50} values were calculated and are presented in **Table 4**. The survival rate of HeLa, A549, K562, MOLT-4, MCF-7, and HUVEC cells after 48 hours of incubation with compound (**1**), (**2**), (dmpbt) and *cis*-Pt are shown in **Figures S5–S10 (Supporting Information)**. These cell lines were chosen arbitrarily and

View Article Online
DOI: 10.1039/C9DT01803D

included cancer (A549, K562 and HeLa) and non-cancerous cells (HUVEC). Cancer cells originated from different tissues, i.e. lung (A549), cervix (HeLa) and blood (K562) and represent solid and blood tumors. In addition, these cells display different growth characteristics, i.e. adherent (A549, HeLa) and suspension (K562) cells.

Table 4. The IC_{50} (mean ± SD) values calculated after 48h incubation of cells with test compounds. The means ± SD are shown

Compound	IC_{50} [μM]					
	HeLa	**K562**	**A549**	**MOLT-4**	**MCF-7**	**HUVEC**
mer-(**1**)	5 ± 0.6	2 ± 0.4	30 ± 5	14 ± 4.4	17 ± 3.3	40 ± 16
fac-(**2**)	26 ± 3.2	26 ± 2.5	5 ± 2.6	19 ± 3.9	16 ± 3.5	4.2 ± 0.56
dmpbt	500 ± 27	800 ± 47	800 ± 29	900 ± 25	800 ± 31	>1000
cis-Pt	20 ± 6	40 ± 7	30 ± 6.5	40 ± 4.0	35 ± 4.7	30 ± 6.5

Compound *mer*-Ru(III) (**1**) showed strong toxicity toward HeLa and K562 cells with IC_{50} values of 5 and 2 μM, respectively. The toxicity of (**1**) against HeLa and K562 was higher that the *fac*-Ru(III) (**2**) (IC_{50} 26 μM) and *cis*-Pt (IC_{50} 20 μM and 40 μM). On the other hand, (**1**) was less toxic toward A549 cells (IC_{50} 30 μM) than (**2**) (IC_{50} 5 μM) but was comparable with *cis*-Pt. Interestingly, *mer*-Ru(III) (**1**) exhibited the least toxicity (IC_{50} 40 μM) against normal endothelial cells when compared to (**2**) and *cis*-Pt. The obtained results suggest that the differences in cytotoxicity of the both isomers are likely related to lipophilicity.

In turn, toxicity of (**1**) and (**2**) toward the MOLT-4 and MCF-7 was comparable, and dmpbt was non-toxic against any of the cell lines (IC_{50} > 500).

View Article Online
DOI: 10.1039/C9DT01803D

According to Alessio,[12] summarising the results of the research on NAMI-A, attention was drawn to the fact that strong cytotoxicity is not always a good feature for determining anticancer properties of a compound. This is confirmed by differences in cytotoxicity *in vitro* and *in vivo* for NAMI-A, KP1019, and RAPTA group. Hence, in case of our complexes ((**1**), (**2**)) the study on the cytotoxic activity *in vivo* and interactions with proteins should be taken into account.

Caspase-3/7 assay

Having demonstrated that ruthenium complexes (**1**) and (**2**) are toxic towards cancer cells (**Table 4**), we investigated whether these compounds induce apoptosis. Experiments were performed in HeLa cells. Cells treated with staurosporine (a strong inducer of activity of caspase 3/7) served as a positive control. As shown in **Figure 8**, in the presence of 1 μM staurosporine the activity of caspase 3/7 increased 6-fold compared to control cells. *Cis*-Pt at 50 μM induced apoptosis in HeLa cells, as evidenced by the 3-fold increase of activity of caspase 3/7. Interestingly, compound (**1**) also activated caspase 3/7, however, to a lesser extent than staurosporine or *cis*-Pt. In the presence of (**1**) (25 μM) the activity of caspase 3/7 was 1.5-fold higher than in control cells. In the cells treated with compound (**2**) (50 μM) we observed a more than 4-fold increase of caspase 3/7 activity, while **dmpbt** had no effect. These results strongly suggest that ruthenium complexes (**1**) and (**2**) induce apoptosis in cancer cells.

View Article Online
DOI: 10.1039/C9DT01803D

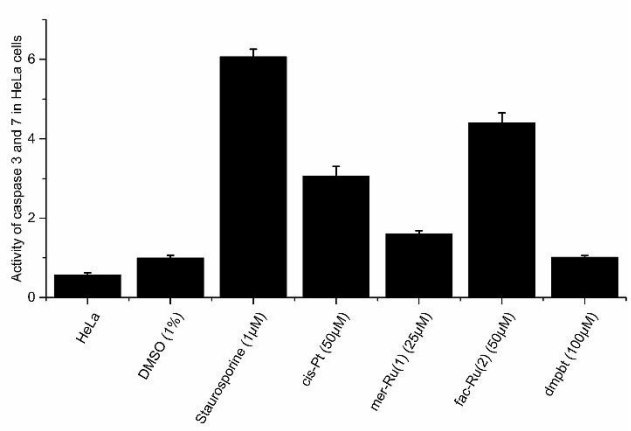

Fig. 8 Activity of caspase 3 and 7 in HeLa cells treated with the test compound (**1**), dmpbt, (**2**), *cis*-Pt or staurosporine for 18h. Apoptosis was determined by Apo-ONE® Homogeneous Caspase-3/7 Assay (Promega, Madison, WI, USA). Abbreviations: HeLa – untreated cells; DMSO – cells treated with 1% DMSO (control). The caspases activity in cells exposed to 1% DMSO was normalized to 1.0. Mean values +/- SD are shown.

The interaction study of compounds (**1**) and (**2**) with DNA was examined by the effect of ruthenium(III) compounds on the conformation of the DNA (circular dichroism) and by digestion of plasmid DNA with BamHI restriction nuclease. Unfortunately, in the presence of the tested compounds no significant changes in DNA spectra impact on the secondary structure of DNA (description in the **Supporting Information**, **Fig. S9, S10**)

CONCLUSIONS

Summarising, two mononuclear *mer*-(**1**) and *fac*-(**2**) ruthenium(III) complexes have been synthesised in the reaction between $[RuCl_3(PPh_3)_3]$ and dmpbt in a 1:1 molar ratio. The appropriate reaction conditions allowed pure geometrical isomers to be obtained without chromatographic separation or fractional crystallisation. The crystal structures of both complexes were solved by

View Article Online
DOI: 10.1039/C9DT01803D

X-ray diffraction methods and showed a slightly distorted octahedral geometry for the Ru(III) centre. The structural change of the *mer*-Ru(III) (**1**) to *fac*-Ru(III) (**2**) isomer is probably caused by structural transformations – "single crystal-to-single crystal" (SCSC). Also, the presence of a suitable acid and non-coordinated binding solvent plays an essential role in the change of *mer* (**1**) to *fac* (**2**) and the generation of *fac* (**2'**) as a first product.

Moreover, the complexes were characterised by infrared spectroscopy, ultraviolet spectroscopy and electron paramagnetic resonance.

Cyclic voltammetric measurements showed redox activity of both isomers and displayed quasi-reversible metal centered redox processes for Ru(III)/Ru(II) and reversible for Ru(IV)/Ru(III) redox couples. The potential of both redox pairs is within the range of physiological cell redox potential. This suggests that the activation process may occur through reduction in a biological environment. However, ruthenium in the +III state is more stable in the coordination sphere of the *fac*- than *mer*-isomer and the mechanism of activation by reduction is based on Ru(III)/Ru(II) redox activity in literature reports.

The log *P* of the *mer*- Ru(III) (**1**) and *fac*-Ru(III) (**2**) values were in the range of the optimal physicochemical properties for drug transport.

Compound (**1**) shows higher toxicity towards HeLa and K562 cancer cells and lower toxicity against normal endothelial cells (HUVEC) than *cis*-Pt and the (**2**). Complex *fac*-Ru(III) (**2**) exhibits higher activity towards A549 than *cis*-Pt.

Compounds (**1**) and (**2**) caused substantial induction of apoptosis in HeLa cells. The pro-apoptotic activity of **(2)** was significantly higher than (**1**) and *cis*-Pt.

The obtained results suggest that the differences in cytotoxicity of the both isomers towards HeLa and K562 cancer cells is likely related to lipophilicity. In the case of the cell lines MOLT

View Article Online
DOI: 10.1039/C9DT01803D

and MCF-7, no similar relationship was observed. Probably another factor determines such a result. The results of the research DNA interactions with *mer*-(**1**) and *fac*-(**2**) ruthenium(III) complexes, showed that DNA is not the primary target for our complexes. Probably the different cytotoxicity of complexes results from targeting specific (yet unidentified) cellular protein(s). It is also possible that our complexes aim different protein(s) depending on the cell line because cell lines differ significantly in the expression of proteins. Further studies are required to defined the molecular targets of the *mer*-(Ru(III) (**1**) and *fac*-(Ru(III) (**2**) isomers, and *in vivo* testing.

ASSOCIATED CONTENT

Supporting Information

Dmpbt characteristic (elemental analysis, IR, ^{1}H NMR) (**Figures S1, S2**). EPR spectrum of (**1**) in solid state (**Figure S3**). Crystal structure description of the *fac*-[$RuCl_3(PPh_3)$(dmpbt)]·C_2H_5OH (**2'**), and its short comparison with (**2**) (**Figure S4**, **Tables S1, S3**). The survival rate of HeLa, A549, K562, MCF-7, MOLT-4 and HUVEC cells after 48 hours of incubation with compound (**1**), (**2**), dmpbt and *cis*-Pt (**Figures S5–S10**). Digestion of plasmid DNA with BamHI restriction nuclease (**Figure S11**). Interaction of (**1**), (**2**), dmpbt, and *cis*-Pt with DNA – circular dichroism (CD) (**Figure S12**). **Figures S1–S12**, **Tables S1 and S3**.

Accession Codes

CCDC 1030325, 1030304, and 1826278 contain the supplementary crystallographic data for this paper. These data can be obtained free of charge via **www.ccdc.cam.ac.uk.**

Conflicts of interest

There are no conflicts to declare.

View Article Online
DOI: 10.1039/C9DT01803D

ACKNOWLEDGEMENTS

The authors wish to acknowledge the Polish National Science Centre for financial support grants no. 2011/03/D/NZ7/02283

REFERENCES

1. S. J. Lippard, *Science*, 1982, **218**, 1075-1082.
2. D. Cocic, S. Jovanovic, S. Rajkovic and B. Petrovic, *Inorganica Chimica Acta*, 2018, **482**, 635-642.
3. P. Starha, J. Vanco and Z. Travnicek, *Coordination Chemistry Reviews*, 2019, **380**, 103-135.
4. M. J. Clarke, F. C. Zhu and D. R. Frasca, *Chemical Reviews*, 1999, **99**, 2511-2533.
5. C. S. Allardyce and P. J. Dyson, *Platinum Metals Review*, 2001, **45**, 62-69.
6. M. A. Jakupec, M. Galanski, V. B. Arion, C. G. Hartinger and B. K. Keppler, *Dalton Transactions*, 2008, 183-194.
7. B. K. Keppler and W. Rupp, *Journal of Cancer Research and Clinical Oncology*, 1986, **111**, 166-168.
8. F. T. Garzon, M. R. Berger, B. K. Keppler and D. Schmahl, *Cancer Chemotherapy and Pharmacology*, 1987, **19**, 347-349.
9. E. Alessio and L. Messori, *Metal ions in life sciences*, 2018, **18**.
10. A. Bergamo and G. Sava, *International Journal of Molecular Sciences*, 2018, **19**, 2.
11. B. G. Dwyer, E. Johnson, E. Cazares, K. L. McFarlane Holman and S. R. Kirk, *Journal of Inorganic Biochemistry*, 2018, **182**, 177-183.
12. E. Alessio, *European Journal of Inorganic Chemistry*, 2017, DOI: 10.1002/ejic.201600986, 1549-1560.
13. S. Leijen, S. A. Burgers, P. Baas, D. Pluim, M. Tibben, E. van Werkhoven, E. Alessio, G. Sava, J. H. Beijnen and J. H. M. Schellens, *Investigational New Drugs*, 2015, **33**, 201-214.
14. B. S. Murray, M. V. Babak, C. G. Hartinger and P. J. Dyson, *Coordination Chemistry Reviews*, 2016, **306**, 86-114.
15. J. Palmucci, F. Marchetti, R. Pettinari, C. Pettinari, R. Scopelliti, T. Riedel, B. Therrien, A. Galindo and P. J. Dyson, *Inorganic Chemistry*, 2016, **55**, 11770-11781.
16. M. Sulyok, S. Hann, C. G. Hartinger, B. K. Keppler, G. Stingeder and G. Koellensperger, *Journal of Analytical Atomic Spectrometry*, 2005, **20**, 856-863.
17. L. S. Flocke, R. Trondl, M. A. Jakupec and B. K. Keppler, *Investigational New Drugs*, 2016, **34**, 261-268.
18. L. Biancalana, G. Pampaloni and F. Marchetti, *Chimia*, 2017, **71**, 573-579.
19. S. Y. Liu, A. H. Liang, K. Wu, W. J. Zeng, Q. Luo and F. Y. Wang, *International Journal of Molecular Sciences*, 2018, **19**, 2137.
20. A. Bergamo and G. Sava, *Dalton Transactions*, 2007, DOI: 10.1039/b617769g, 1267-1272.
21. I. Bratsos, S. Jedner, T. Gianferrara and E. Alessio, *Chimia*, 2007, **61**, 692-697.
22. C. Pelillo, H. Mollica, J. A. Eble, J. Grosche, L. Herzog, B. Codan, G. Sava and A. Bergamo, *Journal of Inorganic Biochemistry*, 2016, **160**, 225-235.

View Article Online
DOI: 10.1039/C9DT01803D

23. K. Spiewak and M. Brindell, *Journal of Biological Inorganic Chemistry*, 2015, **20**, 695-703.
24. L. Biancalana, I. Abdalghani, F. Chiellini, S. Zacchini, G. Pampaloni, M. Crucianelli and F. Marchetti, *European Journal of Inorganic Chemistry*, 2018, DOI: 10.1002/ejic.201800284, 3041-3057.
25. J. Bravo, S. Bolano, L. Gonsalvi and M. Peruzzini, *Coordination Chemistry Reviews*, 2010, **254**, 555-607.
26. R. Pettinari, F. Marchetti, C. Di Nicola, C. Pettinari, A. Galindo, R. Petrelli, L. Cappellacci, M. Cuccioloni, L. Bonfili, A. M. Eleuteri, M. da Silva and A. J. L. Pombeiro, *Inorganic Chemistry*, 2018, **57**, 14123-14133.
27. J. J. Li, Z. Z. Tian, X. X. Ge, Z. S. Xu, Y. Q. Feng and Z. Liu, *European Journal of Medicinal Chemistry*, 2019, **163**, 830-839.
28. E. Alessio, G. Mestroni, A. Bergamo and G. Sava, *Current Topics in Medicinal Chemistry*, 2004, **4**, 1525-1535.
29. I. V. Magedov, M. Manpadi, S. Van slambrouck, W. F. A. Steelant, E. Rozhkova, N. M. Przheval'skii, S. Rogelj and A. Kornienko, *Journal of Medicinal Chemistry*, 2007, **50**, 5183-5192.
30. G. Szabo, J. Fischer, A. Kis-Varga and K. Gyires, *J Med Chem*, 2008, **51**, 142-147.
31. Z. Ozdemir, H. B. Kandilci, B. Gumusel, U. Calis and A. A. Bilgin, *Eur J Med Chem*, 2007, **42**, 373-379.
32. K. K. Sivakumar, A. Rajasekaran, I. Ponnilavarasan, A. Somasundaram, R. Sivasakthi and S. Kamalaveni, *Der Pharmacia Lettre*, 2010, **2**, 211-219.
33. K. Yamazaki, Y. Kaneko, K. Suwa, S. Ebara, K. Nakazawa and K. Yasuno, *Bioorganic & medicinal chemistry*, 2005, **13**, 2509-2522.
34. C. G. Mortimer, G. Wells, J. P. Crochard, E. L. Stone, T. D. Bradshaw, M. F. G. Stevens and A. D. Westwell, *Journal of Medicinal Chemistry*, 2006, **49**, 179-185.
35. R. I. Fryer, P. Zhang, R. Rios, Z. Q. Gu, A. S. Basile and P. Skolnick, *Journal of Medicinal Chemistry*, 1993, **36**, 1669-1673.
36. A. Burger and S. N. Sawhney, *Journal of Medicinal Chemistry*, 1968, **11**, 270-273.
37. R. D. Chakole, N. D. Amnerkar, P. B. Khedekar and K. P. Bhusari, *Indian Journal of Heterocyclic Chemistry*, 2005, **15**, 27-30.
38. N. Siddiqui, M. Alam and A. A. Siddiqui, *Asian Journal of Chemistry*, 2004, **16**, 1005-1008.
39. B. M. Gurupadayya, M. Gopal, B. Padmashali and V. P. Valdya, *Indian Journal of Heterocyclic Chemistry*, 2005, **15**, 169-172.
40. M. Sobiesiak, K. Sobiesiak, A. Mrozek, P. Mayer, I. P. Lorenz, M. Rozalski, U. Krajewska and E. Budzisz, *Inorganica Chimica Acta*, 2010, **363**, 2171-2179.
41. M. Sobiesiak, I. P. Lorenz, P. Mayer, M. Wozniczka, A. Kufelnicki, U. Krajewska, M. Rozalski and E. Budzisz, *European Journal of Medicinal Chemistry*, 2011, **46**, 5917-5926.
42. N. R. Pramanik, S. Ghosh, T. K. Raychaudhuri, M. G. B. Drew, T. K. Mandal and S. S. Mandal, *Inorganica Chimica Acta*, 2012, **383**, 60-66.
43. A. Sharma, J. F. Arambula, S. Koo, R. Kumar, H. Singh, J. L. Sessler and J. S. Kim, *Chemical Society Reviews*, 2019, **48**, 771-813.
44. P. Schluga, C. G. Hartinger, A. Egger, E. Reisner, M. Galanski, M. A. Jakupec and B. K. Keppler, *Dalton Trans.*, 2006, 1796-1802.

View Article Online
DOI: 10.1039/C9DT01803D

45. V. K. Revankar, V. H. Arali and V. B. Mahale, *Indian Journal of Chemistry Section a-Inorganic Bio-Inorganic Physical Theoretical & Analytical Chemistry*, 1990, **29**, 889-894.
46. J. Chatt, G. J. Leigh, D. M. P. Mingos and R. J. Paske, *Journal of the Chemical Society A: Inorganic, Physical, Theoretical*, 1968, DOI: 10.1039/J19680002636, 2636-2641.
47. B. N. Figgis, R. S. Nyholm, D. Nasipuri, B. E. Betts, W. Davey, M. A. P. Hogg, J. E. Spice, E. Boyland, P. Sims, M. M. Coombs, J. Lamy, D. Lavit, N. P. Buu-Hoi, S. J. W. Price, A. F. Trotman-Dickenson, D. J. Alner, A. G. Smeeth, W. Tadros, A. B. Sakla, M. S. Ishak, F. C. Cooper, C. L. Arcus, P. A. Hallgarten and D. A. H. Taylor, *Journal of the Chemical Society (Resumed)*, 1958, 4190-4216.
48. E. König, *Magnetic Properties of Coordination and Organometallic Transition Metal Compounds*, Springer-Verlag Berlin Heidelberg, Berlin, 1966.
49. *CrysAlis RED and CrysAlis CCD*. 2000, Oxford Diffraction Ltd.: Abingdon, Oxfordshire, England.
50. G. M. Sheldrick, *Acta Crystallographica Section A*, 2008, **64**, 112-122.
51. K. Brandenburg, *Diamond*. 2001, Crystal Impact GbR: Bonn, Germany.
52. L. Farrugia, *Journal of Applied Crystallography*, 1997, **30**, 565.
53. A. L. Spek, *Acta Crystallographica Section D-Biological Crystallography*, 2009, **65**, 148-155.
54. M. Walczyk, A. Świątkowski, M. Pakuła and S. Biniak, *Journal of Applied Electrochemistry*, 2005, **35**, 123-130.
55. OECD, *Test No. 107: Partition Coefficient (n-octanol/water): Shake Flask Method*, 1995.
56. M. H. M. Klose, S. Theiner, H. P. Varbanov, D. Hoefer, V. Pichler, M. Galanski, S. M. Meier-Menches and B. K. Keppler, *Inorganics*, 2018, **6**(4), 130.
57. M. Maszewska, J. Leclaire, M. Cieslak, B. Nawrot, A. Okruszek, A. M. Caminade and J. P. Majoral, *Oligonucleotides*, 2003, **13**, 193-205.
58. S. L. Dabb and N. C. Fletcher, *Dalton Transactions*, 2015, **44**, 4406-4422.
59. N. C. Fletcher, M. Nieuwenhuyzen and S. Rainey, *Journal of the Chemical Society-Dalton Transactions*, 2001, 2641-2648.
60. G. Von Poelhsitz, M. P. de Araujo, L. A. A. de Oliveira, S. L. Queiroz, J. Ellena, E. E. Castellano, A. G. Ferreira and A. A. Batista, *Polyhedron*, 2002, **21**, 2221-2225.
61. G. Von Poelhsitz, R. C. de Lima, R. M. Carlos, A. G. Ferreira, A. A. Batista, A. S. de Araujo, J. Ellena and E. E. Castellano, *Inorganica Chimica Acta*, 2006, **359**, 2896-2909.
62. J. P. da Silva, F. R. Caetano, D. A. Cavarzan, F. D. Fagundes, L. L. Romualdo, J. Ellena, M. Jaworska, P. Lodowski, A. Barison and M. P. de Araujo, *Inorganica Chimica Acta*, 2011, **373**, 8-18.
63. N. C. Fletcher, M. Nieuwenhuyzen, R. Prabarahan and A. Wilson, *Chemical Communications*, 2002, 1188-1189.
64. E. A. P. Armstrong, R. T. Brown, M. S. Sekwale, N. C. Fletcher, X. Q. Gong and P. Hu, *Inorganic Chemistry*, 2004, **43**, 1714-1722.
65. K. S. Lim, D. W. Ryu, W. R. Lee, E. K. Koh, H. C. Kim and C. S. Hong, *Chemistry-a European Journal*, 2012, **18**, 11541-11544.
66. L. Aboutorabi and A. Morsali, *Coordination Chemistry Reviews*, 2016, **310**, 116-130.
67. M. L. Sun, L. Zhang, Q. P. Lin, J. Zhang and Y. G. Yao, *Crystal Growth & Design*, 2010, **10**, 1464-1467.
68. A. Garza-Ortiz, P. U. Maheswari, M. Siegler, A. L. Spek and J. Reedijk, *New Journal of Chemistry*, 2013, **37**, 3450-3460.

View Article Online
DOI: 10.1039/C9DT01803D

69. R. Raveendran and S. Pal, *Inorganica Chimica Acta*, 2006, **359**, 3212-3220.
70. K. Nakamoto, in *Infrared and Raman Spectra of Inorganic and Coordination Compounds*, John Wiley & Sons, Inc., 2008, pp. 149-354.
71. F. Basuli, A. K. Das, G. Mostafa, S. M. Peng and S. Bhattacharya, *Polyhedron*, 2000, **19**, 1663-1672.
72. H. O. Desseyn, M. Hereygers and S. P. Perlepes, *Journal of Raman Spectroscopy*, 1995, **26**, 77-82.
73. O. K. Medhi and U. Agarwala, *Inorganic Chemistry*, 1980, **19**, 1381-1384.
74. A. B. P. Lever, *Inorganic electronic spectroscopy*, Elsevier, Amsterdam; New York, 1984.
75. M. J. Clarke, S. Bitler, D. Rennert, M. Buchbinder and A. D. Kelman, *Journal of Inorganic Biochemistry*, 1980, **12**, 79-87.
76. E. I. Rogers, D. S. Silvester, D. L. Poole, L. Aldous, C. Hardacre and R. G. Compton, *Journal of Physical Chemistry C*, 2008, **112**, 2729-2735.
77. A. Jablonska-Wawrzycka, P. Rogala, S. Michalkiewicz, M. Hodorowicz and B. Barszcz, *Dalton Transactions*, 2013, **42**, 6092-6101.
78. M. Ravera, C. Cassino, S. Baracco and D. Osella, *European Journal of Inorganic Chemistry*, 2006, DOI: 10.1002/ejic.200500634, 740-746.
79. F. Q. Schafer and G. R. Buettner, *Free Radical Biology and Medicine*, 2001, **30**, 1191-1212.
80. B. Lippert (Ed.), Cisplatin, Chemistry and Biochemistry of a Leading Anticancer Drug, Wiley-VCH, Weinheim, 1999.
81. A. F. Westendorf, L. Zerzankova, L. Salassa, P. J. Sadler, V. Brabec and P. J. Bednarski, *Journal of Inorganic Biochemistry*, 2011, **105**, 652-662.
82. C. Vraka, L. Nics, K.-H. Wagner, M. Hacker, W. Wadsak and M. Mitterhauser, *Nuclear Medicine and Biology*, 2017, **50**, 1-10.
83. Y. Gao, C. Gesenberg and W. Zheng, *Oral Formulations for Preclinical Studies: Principle, Design, and Development Considerations*, Academic Press Ltd-Elsevier Science Ltd, London, 2017.
84. S. W. Chang, A. R. Lewis, K. E. Prosser, J. R. Thompson, M. Gladkikh, M. B. Bally, J. J. Warren and C. J. Walsby, *Inorganic Chemistry*, 2016, **55**, 4850-4863.
85. J. Masternak, A. Gilewska, K. Kazimierczuk, O. V. Khavryuchenko, J. Wietrzyk, J. Trynda and B. Barszcz, *Polyhedron*, 2018, **154**, 263-274.

TOC

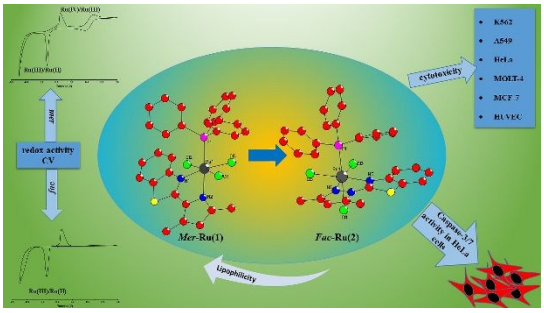

View Article Online
DOI: 10.1039/C9DT01803D

Chemical characterization and biological activity of the pure *mer*- and *fac*-Ru(III) geometrical isomers bearing 2-(3,5-dimethylpyrazol-1-yl)benzothiazole (dmpbt).